Blue Shift of Localized Surface Plasmon Resonance of Gold Ultrathin Nanorod by Forming a Single Atomic Silver Shell via Antigalvanic Process

Subarna Maity,[1] Toshiki Komagata,[1] Shinjiro Takano,[1] Shinya Masuda,[1] Jun Kikkawa,[2] Koji Kimoto,[2] Koji Harano*[2] and Tatsuya Tsukuda*[1]

[1]Department of Chemistry, Graduate School of Science, The University of Tokyo, 7-3-1 Hongo, Bunkyo-ku, Tokyo 113-0033, Japan

[2]Center for Basic Research on Materials, National Institute for Materials Science, 1-1 Namiki, Tsukuba, Ibaraki 305-0044, Japan

ABSTRACT: Gold ultrathin nanorods (Au UNRs) are anisotropic nanostructures constructed by attaching gold nanoclusters in one dimension. Au UNRs exhibit localized surface plasmon resonance (LSPR) only in the longitudinal direction because their diameter is smaller than the Fermi wavelength of an electron (<2 nm). In this study, we found that the LSPR wavelength of oleylamine-stabilized Au UNRs is blue shifted simply by mixing with Ag(I). High-resolution elemental mapping and X-ray photoemission spectroscopy of the resulting UNRs indicate that an Ag monoatomic layer is formed on the Au UNR surface by the antigalvanic reduction of Ag(I). This process allowed us to synthesize a series of Au@Ag core-shell UNRs with LSPR wavelengths in the range of 1.2–2.0 μm.

Keywords: Gold Ultrathin Nanorod, Localized Surface Plasmon Resonance, Au@Ag Core-Shell Structure, Antigalvanic Reaction

Anisotropic gold nanostructures have attracted considerable research interest for the wide range of photonic and biological applications exploiting the unique plasmonic properties.[1, 2] Among others, gold nanorods (Au NRs) with diameters and lengths larger than a few tens of nanometers exhibit distinct transverse and longitudinal modes of localized surface plasmon resonance (LSPR), which arise from the collective oscillation of free electrons under electromagnetic irradiation. The longitudinal LSPR mode is red shifted with increasing aspect ratio (AR) of the NRs, while the transverse LSPR remains almost unchanged regardless of the diameter. Tuning the LSPR with AR is highly desirable for applications in sensing, photovoltaics, bioimaging, therapeutics.[3-5] Meanwhile, a new class of rod-like Au nanoclusters (NCs) with diameter smaller than the Fermi wavelength of electrons (<2 nm) has recently emerged: the examples include $[Au_{37}(SR)_{10}(PPh_3)_{10}Cl_2]^+$,[6] $Au_{38}(SR)_{24}$,[7] $Au_{42}(SR)_{32}$,[8] $Au_{76}(SR)_{44}$,[9] $Au_{64}(SR)_{44}$,[10] $Au_{60}(SR)_{44}$,[11] $Au_{78}(SR)_{56}$,[11] $Au_{96}(SR)_{68}$,[11] and $Au_{114}(SR)_{80}$,[11] where RS represents thiolate. They exhibit an optical absorption peak in the NIR region (815–1700 nm). These peaks are not assigned to the LSPR band, but to single electron optical transitions between the quantized orbitals.

Gold ultrathin nanorods (Au UNRs) with a diameter of 1.6–2.0 nm occupy a unique position located between plasmonic Au NRs and rod-like Au NCs.[12, 13] Xia first synthesized Au UNRs with AR ~ 30 by reducing AuCl(OA) (OA = oleylamine) with Fe NPs.[14] Kawai and coworkers used long alkyl chain amidoamines and carboxylic acids to synthesize Au ultrathin nanowires.[15, 16] Later, Tsukuda and coworker synthesized Au UNRs with controlled AR in the range of 2.6–15 by one-dimensional oriented attachment of spherical Au NCs in the OA micelle.[12, 17] They exhibit the longitudinal LSPR with large molar extinction coefficient ($2–8 \times 10^6$ $M^{-1}cm^{-1}$) while the transverse LSPR is absent in Au UNRs due to the small diameter.[17] The longitudinal LSPR wavelength of Au UNRs has been varied in the range of 1.3–2.2 μm by changing the AR. Considering the potential bioapplication of Au UNRs,[18, 19] it is desirable to tune the LSPR to the second biologically transparent window (1.0–1.3 μm) in the NIR-II region. However, it is a synthetic challenge to further blue shift the LSPR band by reducing the AR. Alternatively, Tsukuda achieved the blue shift of the LSPR wavelength by surface modification with thiolate on the OA-coated Au UNR.[17]

Another promising method to blue shift the LSPR of Au UNRs is the introduction of silver (Ag) atoms. The longitudinal LSPR band of Au@Ag core-shell NRs was gradually blue shifted with increasing Ag shell thickness.[20, 21] A discrete dipole approximation simulation based on a confocal ellipsoid model qualitatively reproduced the spectral shift using dielectric functions of bulk Au and Ag. These results suggest that the LSPR of the Au UNRs can be blue shifted by Ag sheathing.

Recently, a novel reaction called antigalvanic reaction (AGR) has gained considerable interest as a new synthetic method for alloy NPs and NCs.[22-25] In AGR, metal ions are reduced by less reactive (or noble) metals, which is the reverse of the conventional galvanic reaction and is specifically observed with small (< 3 nm) metal NPs. Murray was the first to find that the Ag^+ ions are reduced by $Au_{25}(SR)_{18}$ to form $Ag_xAu_{25-x}(SR)_{18}$.[26] Wang reported that more Ag is introduced into smaller Au NPs.[27] Zamborini demonstrated that the Au NCs (0.9 nm) supported on a glass/ITO electrode are completely replaced by Ag.[28] The occurrence of the AGR on smaller Au NPs is attributed to a decrease in oxidation potential (i.e., enhanced reducing ability). In fact, Ag^+ ions are spontaneously reduced on the surface of small Au NPs or NCs, while those adsorbed on larger Au NPs by underpotential deposition are not reduced.[29, 30] Unique features of the AGR-based synthesis are (1) preferential formation of Au@Ag core-shell NPs;[28,31] and (2) easy control of the amount of Ag dopants by simply changing the concentration of Ag^+ precursors.

AGR is a promising approach for controlled doping Ag on the surface of Au UNRs. However, it is not clear whether it is applicable to Au UNRs since their lengths are far beyond the critical size for AGR (~3 nm). In this study, we attempted to deposit Ag atoms on OA-stabilized Au UNRs by reaction with

Ag^+ ions in solution. The resulting AuAg bimetallic UNRs had monodisperse morphologies with ARs ranging from 12.4 to 4.7. High-resolution elemental mapping analyses revealed the formation of an almost single atomic layer of Ag on the surface of Au UNRs. The LSPR wavelengths of Au@Ag core-shell UNRs were in the range of 1.95 to 1.19 μm, blue shifted by ~300 nm with respect to those of Au UNRs with nearly the same AR. This work provides a facile and powerful method to introduce Ag on the surface of Au UNRs to tune the plasmonic properties for future applications.

A series of Au UNRs **1**–**4** with decreasing ARs were prepared according to the previous report with slight modifications (see Supporting Information for details). Figure 1a shows the images obtained by transmission electron microscopy (TEM) and geometric factors (lengths and diameters) of **1**–**4** obtained from the analysis of >500 particles. Additional TEM images and length and diameter distribution plots are shown in Figures S1 and S2, respectively. The ARs of **1**–**4** are estimated to be 13.2 ± 3.8, 10.0±3.5, 7.6±3.3, and 5.9±2.6, respectively. The longitudinal LSPR wavelengths of **1**–**4** are determined to be 2.30, 1.87, 1.58, and 1.50 μm, respectively, by UV-Vis-NIR optical spectroscopy (red traces in Figure 1b): the LSPR wavelength of **1** was determined by measuring the spectrum of a drop-cast film on a CaF_2 plate to

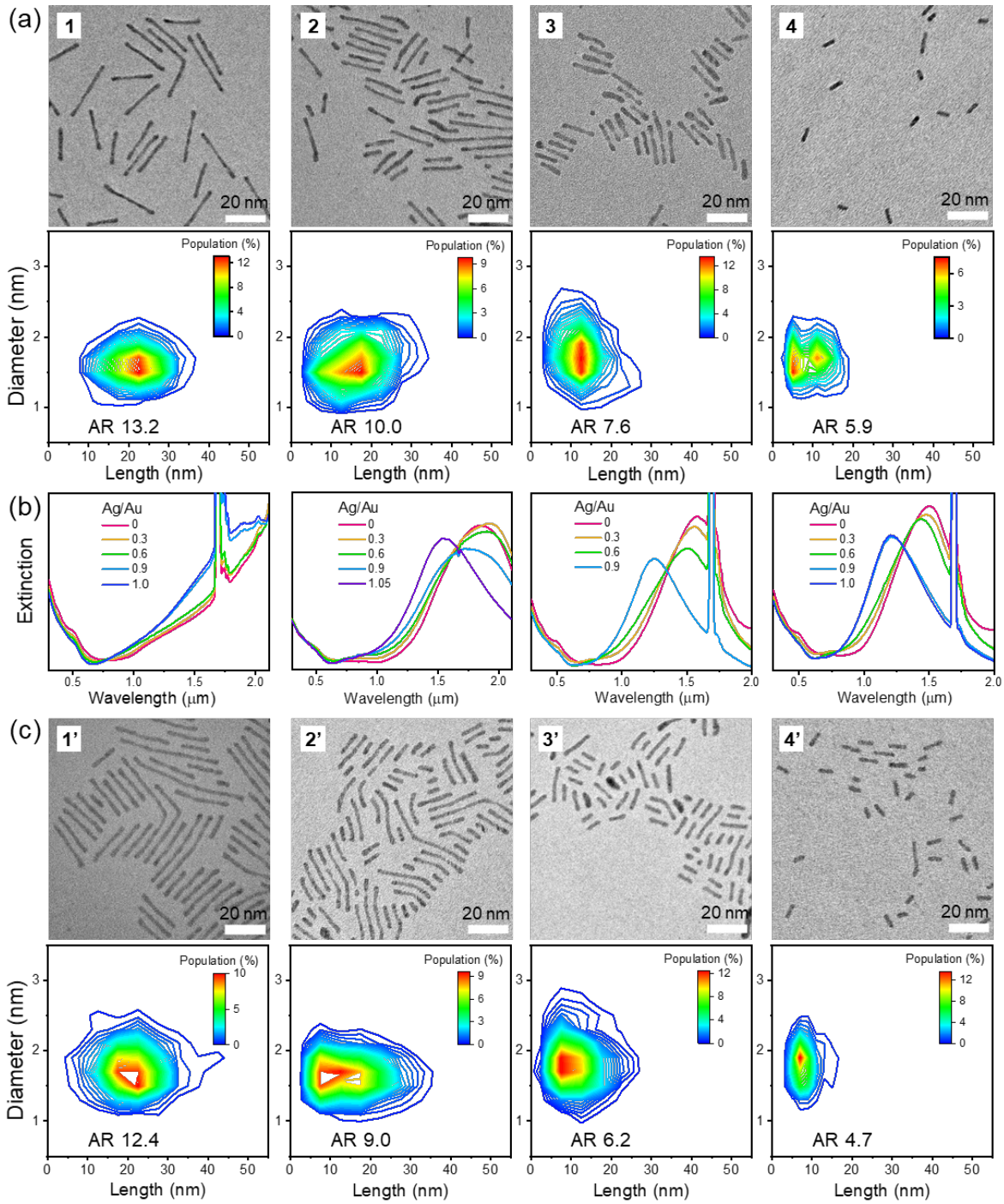

Figure 1: (a) TEM images (top panels) and aspect ratio distributions (bottom panels) of **1**–**4**, (b) UV-Vis-NIR extinction spectra recorded by adding increasing amounts of $AgCF_3CO_2$ to **1**–**4**, (c) TEM images (top panels) and aspect ratio distributions (bottom panels) of **1'**–**4'**. The intense peak at 1.68 μm in the optical spectra is assigned to the CH stretching overtone band of toluene. This peak is almost absent in the extinction spectra for the mixtures of **2** and $AgCF_3CO_2$ which were recorded in a cuvette with a path length of 2 mm.

avoid interference from strong absorption of the toluene solvent (Figure S3a).

Then, a toluene solution of silver trifluoroacetate ($AgCF_3CO_2$) containing an excess of OA was added to the dispersion of Au UNRs at a controlled rate (see SI for details). Figure 1b shows the UV-Vis-NIR extinction spectra of the reaction mixtures of **1**–**4** as a function of the molar ratio of Ag and Au atoms in the mixture. Figure 1b shows that the LSPR band was gradually blue shifted, while the extinction decreases slightly with increasing amount of Ag^+ added: the effect of the dilution on the extinction decrease is negligible, considering that the dilution factor is only 0.5% at Ag/Au = 0.3. Upon addition of a nearly 1 equiv. of Ag^+, the LSPR wavelength of **1**–**4** is rapidly blue shifted to 1.95, 1.57, 1.25, and 1.19 μm, respectively (Figure 2). The UNRs thus prepared are hereafter referred to as **1'**–**4'**. The spectrum of **1'** with reduced interference from the toluene solvent is shown in Figure S3b, which was recorded using a cuvette with a path length of 2 mm. The reaction products obtained by the reaction with 1 equiv. of Ag^+ remained stable: the extinction spectrum of **4'**, for example, showed no appreciable change over time (Figure S4a) and upon further addition of Ag^+ (Figure S4b). Hence, the rapid blue shift of LSPR marks the completion of the reaction.

The blue shift of the LSPR shows that the reaction with Ag^+ extends the tunability of the LSPR band of Au UNRs into the second biologically transparent window (1.0–1.3 μm) in the NIR-II region. To investigate whether the spectral shift upon Ag^+ addition is related to the morphological change of the UNRs**,** the morphology of **1'**–**4'** was examined by TEM. Figure 1c shows the TEM micrographs of **1'**–**4'**, together with the corresponding AR distribution plots. The TEM images confirm that the rod-shaped morphology is maintained during the reaction with Ag^+. The yield of rod-shaped morphology exceeds 90 % (Table S1). Spherical particles, seen as a minority, may result from the decomposition on the TEM grid considering the fragile nature of UNRs.[32] The high-resolution TEM observation of **1'** shows the twinned crystalline grains similar to the monometallic Au UNRs (Figure S5). The high-angle annular dark-field scanning transmission electron microscopy (HAADF-STEM) images of **1'** and **3'** are shown in Figures S6a and S6b, respectively. The atomic column of Au shown in Figure S6c indicates that the multiply twinned crystallinity is retained. This result suggests that **1'**–**4'** can be considered as a one-dimensional assembly of cuboctahedral particles connected

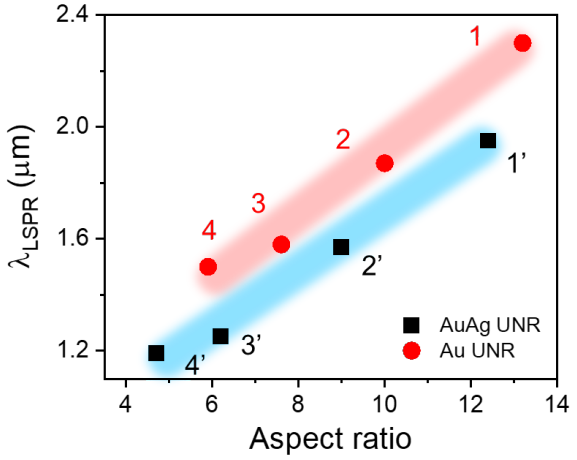

Figure 2: Peak position of the LSPR bands of **1**–**4** (red circles) and **1'**–**4'** (black squares) as a function of their aspect ratio.

by twin boundaries, as in the case of OA-stabilized Au UNRs.[33]

Histograms of the length and diameter are provided in the SI (Table S1 and Figure S2). The average lengths of **1'**–**4'** vary from 21.1 (for **1'**) to 8.3 nm (for **4'**), while the average diameters of **1'**–**4'** remain similar (1.7–1.8 nm). The ARs for **1'**–**4'** are 12.4±3.9, 9.0±2.8, 6.2±2.6, and 4.7±1.7, respectively, which are slightly smaller than those of the corresponding Au UNRs **1**–**4** (13.2, 10.0, 7.6, and 5.9, respectively). According to the correlation between the LSPR wavelength and AR of **1**–**4** (Figure 2), the observed blue shift in **1'**–**4'** cannot be explained by the reduction of AR alone.

The above argument suggests the possibility that the blue shift of the LSPR in **1'**–**4'** is related to the incorporation of Ag. To test such a possibility, we performed high-resolution elemental mapping of a single UNR from representative samples of **1'** and **3'** by energy-dispersive X-ray spectroscopy (EDS). The left column of Figure 3a shows the HAADF-STEM image of a single UNR (length (L) = 14.4 nm; diameter (D) = 2.0 nm) randomly selected from sample **1'**. The elemental maps of Ag and Au and their overlay on the UNR are shown in the left column of Figure 3b. These elemental maps clearly show that the Ag atoms are indeed present in the final UNR. The atomic percentage of Ag is estimated to be 38.6±2.0% by averaging those of eight UNRs randomly selected from sample **1'**. More interestingly, Ag atoms are not randomly distributed in the UNR, but form a shell on the Au UNR. The thickness of the Ag shell around the Au core was estimated from the line scan profiles along the D and L directions. To improve the signal-to-noise ratio, the line scan profile along the D and L axes was obtained by accumulating the signals from the areas shown in the yellow and green frames, respectively (Figure 3c). The full-width at half-maximum (FWHM) of the line profile for Ag, W_{Ag} (2.04 nm) is 0.50 nm larger than that of Au, W_{Au} (1.54 nm) along the D axis. The W_{Ag} (14.44 nm) is 0.24 nm larger than W_{Au} (14.20 nm) along the L axis. Considering the diameter of the silver atom (0.288 nm), the Ag shell thickness estimated from $0.5 \times (W_{Ag} - W_{Au}) / 0.288$ was at most a single atomic layer for sample **1'**. From sample **3'**, we selected a UNR with L = 11.0 nm and D = 2.8 nm as shown in the HAADF-STEM image (right column of Figure 3a). Similarly, the elemental maps of Au and Ag and their overlay (right column of Figure 3b) confirm the formation of Au@Ag core-shell structure. The average atomic percentage of Ag for four UNRs randomly selected from sample **3'** was 30.1±3.4%. The line scan profiles along the short and long axes are shown in the right column of Figure 3c. The W_{Ag} (2.84 nm) is 0.86 nm larger than W_{Au} (1.98 nm) along the D axis, while W_{Ag} (10.98 nm) is 0.73 nm larger than W_{Au} (10.25 nm) along the L axis. These results suggest that the Ag shell thickness for sample **3'** is 1.3–1.5 atomic layers. The high-resolution elemental mapping analyses led us to conclude that Au@Ag core-shell UNRs are spontaneously formed simply by mixing Au UNRs with $AgCF_3CO_2$. The core-shell structure reported here is in contrast to randomly alloyed AuAg UNRs and UNWs formed by the thermal decomposition of organometallic Au-Ag complexes[34, 35] or coreduction of gold and silver salts.[36] Blue shift in the LSPR band was also reported for thicker Au@Ag core-shell NRs.[20, 21] Discrete dipole approximation simulation revealed that this blue shift induced by the Ag coating is explained by the reduction of the electron density in the Au NR.[37] We believe in the similar origin of the blue shift observed in the Au@Ag UNRs.

A naive question is how $AgCF_3CO_2$ forms an almost single atomic layer of Ag on the surface of Au UNR in the absence of any reducing agent. According to recent reports, small Au NCs undergo AGR with metal cations Ag^+, Cu^{2+}, Pb^{2+}, Cd^{2+}, etc.[23] Therefore, a possible explanation for the present observation

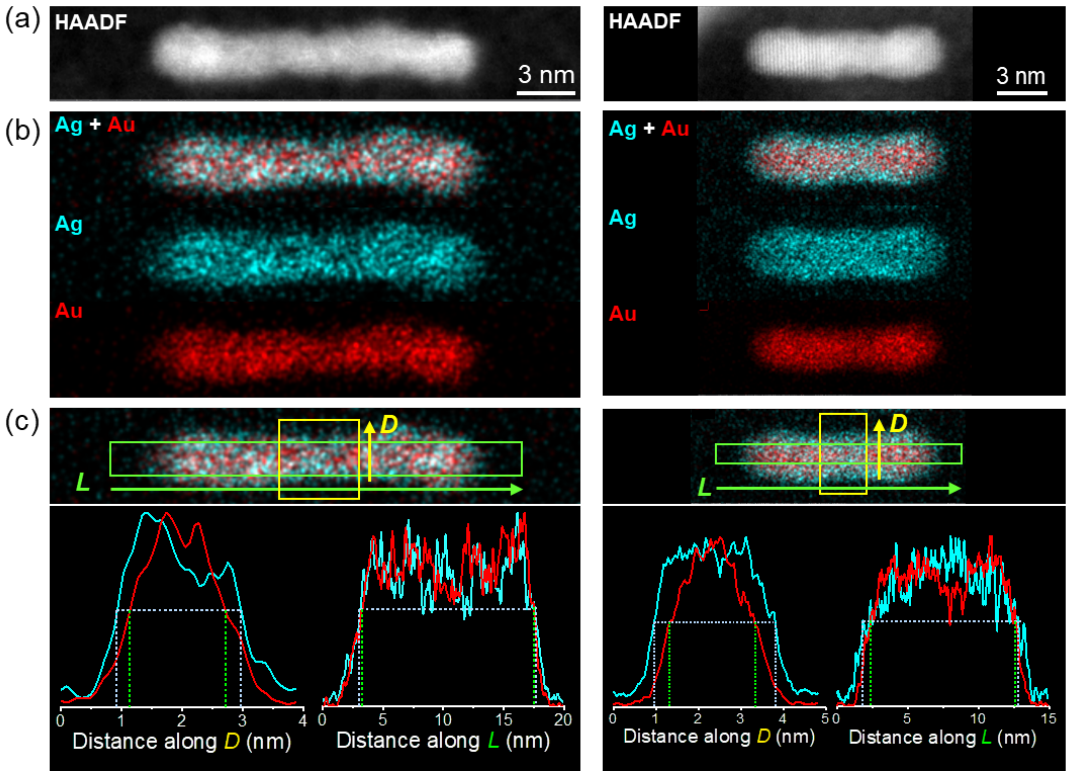

Figure 3: (a) HAADF-STEM images, (b) elemental mapping images of Ag, Au, and overlay, (c) line scan of Ag and Au along the diameter (*D*) and length (*L*) of **1'** (left column) and **3'** (right column). In panel (c), the intensities of each element in the yellow and green boxes are accumulated along *D* and *L*, respectively.

could be the AG reduction of Ag^+ ions on the surface of Au UNRs. Zamborini showed that the Ag^+ ions replaced Au atoms of the Au NPs stabilized with weakly coordinating ligands. The extent of Ag incorporation increased from 17.8 to 100 % as the size of the NPs decreased from 4.1 nm to 0.9 nm.[28] This was explained by the decrease in the oxidation potential of Au NPs with decreasing size.[28] Since the Au UNRs can be considered as a linear assembly of Au NPs of < 2 nm, the oxidation potential of the surface Au atoms may be lower than that of the bulk Au. The negligible difference in diameter (< 0.15 nm) between the original Au UNRs **1**–**4** and Au@Ag UNRs **1'**–**4'** supports the AG reduction followed by the replacement process rather than the simple deposition of Ag.

To confirm the occurrence of the AGR process, two experiments were performed. First, the charge state of Ag in Au@Ag UNRs was investigated by X-ray photoelectron spectroscopy (XPS). The dispersion of Au@Ag UNRs **3'**, obtained by mixing Au UNR (**3**) and 1.0 equiv. of Ag^+, was drop-cast on carbon paper. Figure 4a compares the Ag XP spectra of **3'** and $AgCF_3CO_2$ reactants. The Ag $3d_{5/2}$ and $3d_{3/2}$ binding energies (BEs) of $AgCF_3CO_2$ were determined to be 368.1 and 374.1 eV, which are assigned to Ag(I). On the other

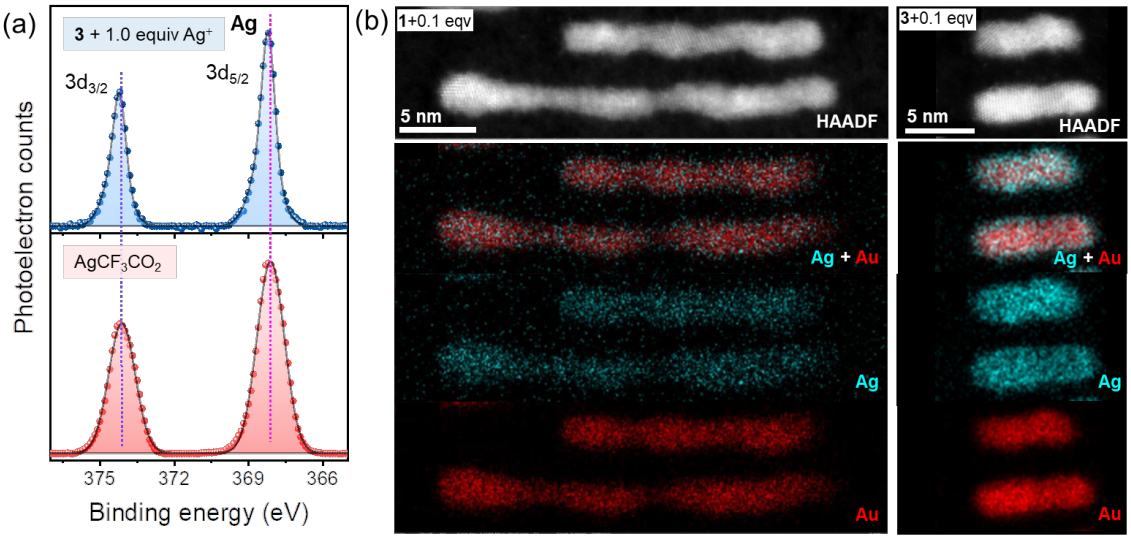

Figure 4: (a) Ag 3d XP spectra of $AgCF_3CO_2$ (bottom panel) and mixture of sample **3** and 1.0 equiv. of Ag^+ (top panel). (b) HAADF-STEM images and EDS elemental maps of Ag and Au of UNRs prepared by mixing **1** (left) and **3** (right) with 0.1 equiv. of Ag^+.

hand, the corresponding Ag 3d peaks for **3'** in the top panel of Figure 4a are shifted to the higher BEs of 368.2 and 374.2 eV. This small energy shift of 0.1 eV is corroborated by the reproducibility of the results with other batch samples and the typical energy ambiguity of 0.03 eV. The shift to the higher BEs supports that Ag^+ ions are reduced by the AGR process. Second, we performed inductively coupled plasma mass spectrometry (ICP-MS) to detect Au(I) species released by the AGR (Au(0) + Ag(I) → Au(I) + Ag(0)), presumably in the form of Au(I)-OA complex (see SI for details). The amount of Au species released into the solutions of **1** increased by 0.22 and 0.38 nmol, respectively, by adding 0.15 and 0.30 equiv. of Ag^+ (Figure S7). These results indicate that the Au atoms of Au UNRs are dissolved in association with AG reduction of Ag^+ ions. To further confirm the occurrence of AGR even when the concentration of Ag^+ is far below the critical value, we performed STEM-EDS elemental mapping on the individual UNRs of **1** and **3** treated with 0.1 equiv. of Ag^+. The elemental maps of Au and Ag shown in Figure 4b clearly indicate that Ag is present on the Au UNR surface.

The question then arises as to why the extinction spectra of **1'**–**4'** underwent a sudden blue shift of 330–300 nm compared to **1**–**4** when the Ag^+ concentration reached the critical value (~1 equiv. with respect to the total Au atoms) (Figure 1b). Considering that the AGR occurred even at the low Ag^+ concentration (Figure 4b and S7), small amount of Ag atoms doped on Au UNR resulted in only a slight blue shift of the LSPR wavelength. In this context, we propose that the sudden blue shift is associated with the completion of an almost monoatomic layer of Ag on Au UNRs. The total surface areas for **1**–**4** were estimated to be approximately the same as the surface area at both ends of the UNRs are very small compared to the total surface area. Thus, the nearly identical amount of Ag^+ required to complete the monoatomic shell formation suggests that the AG reactivity of **1**–**4** are comparable regardless of the AR. Since Au UNR can be modeled as a one-dimensional oligomer of cuboctahedral Au_{147} equivalent units linked via twinning defects,[33] the above conclusion is explained in terms of the AGR reactivity being dominated by the constituent units.

In summary, we have synthesized a series of core-shell Au@Ag UNRs with LSPR in the NIR range (1.95 to 1.19 μm) with aspect ratio varying from 12.4 to 4.7. The plasmon shape correlation curve for the Au@Ag UNRs reveals the high energy shift of the LSPR mode after silver shell formation. Interestingly, the silver shell formation is spontaneous and self-limited to the monoatomic layer around the Au core. The controlled synthesis and establishment of the structure-property relationship of the bimetallic UNRs reported here will promote the development of novel anisotropic nanomaterials with desirable plasmonic behavior.

ASSOCIATED CONTENT

The Supporting Information is available free of charge at http://pubs.acs.org.

Details of syntheses and characterization methods, TEM images of Au and AuAg UNRs, Aspect ratio distribution, tabulated morphological parameters, Extinction spectra of Au and AuAg UNR, HRTEM image of AuAg UNR, HAADF-STEM images of AuAg UNRs, ICP-MS results.

AUTHOR INFORMATION

Corresponding Authors

Tatsuya Tsukuda – Department of Chemistry, Graduate School of Science, The University of Tokyo, 7-3-1 Hongo, Bunkyo-ku, Tokyo 113-0033, Japan; https://orcid.org/0000-0002-0190-6379

E–mail: tsukuda@chem.s.u-tokyo.ac.jp

Koji Harano – Center for Basic Research on Materials, National Institute for Materials Science,1-1 Namiki, Tsukuba, Ibaraki 305-0044, Japan; https://orcid.org/0000-0001-6800-8023

E–mail: harano.koji@nims.go.jp

Authors

Subarna Maity – Department of Chemistry, Graduate School of Science, The University of Tokyo, 7-3-1 Hongo, Bunkyo-ku, Tokyo 113-0033, Japan; https://orcid.org/0000-0002-7118-3591

Toshiki Komagata – Department of Chemistry, Graduate School of Science, The University of Tokyo, 7-3-1 Hongo, Bunkyo-ku, Tokyo 113-0033, Japan.

Shinjiro Takano – Department of Chemistry, Graduate School of Science, The University of Tokyo, 7-3-1 Hongo, Bunkyo-ku, Tokyo 113-0033, Japan; https://orcid.org/0000-0001-9262-5283

Shinya Masuda – Department of Chemistry, Graduate School of Science, The University of Tokyo, 7-3-1 Hongo, Bunkyo-ku, Tokyo 113-0033, Japan; https://orcid.org/0000-0002-6319-3503

Jun Kikkawa – Center for Basic Research on Materials, National Institute for Materials Science, 1-1 Namiki, Tsukuba, Ibaraki 305-0044, Japan; https://orcid.org/0000-0003-0659-1844

Koji Kimoto – Center for Basic Research on Materials, National Institute for Materials Science, 1-1 Namiki, Tsukuba, Ibaraki 305-0044, Japan; https://orcid.org/0000-0002-3927-0492

Notes

The authors declare no competing financial interest.

ACKNOWLEDGMENTS

This research was supported financially by JST, CREST (Grant No. JPMJCR20B2) and partly by JSPS KAKENHI (Grant No. JP23H04874). This work was supported by "Advanced Research Infrastructure for Materials and Nanotechnology in Japan (ARIM)" of the Ministry of Education, Culture, Sports, Science and Technology (MEXT) (Grant No. JPMXP1223UT0082). This research is supported by Grant-in-Aid for JSPS Fellows (Grant No. 23KF0198).

REFERENCES

(1) Li, N.; Zhao, P.; Astruc, D. Anisotropic Gold Nanoparticles: Synthesis, Properties, Applications, and Toxicity. *Angew. Chem., Int. Ed.* **2014**, *53* (7), 1756–1789.

(2) Yoo, S.; Go, S.; Son, J.; Kim, J.; Lee, S.; Haddadnezhad, M.; Hilal, H.; Kim, J.-M.; Nam, J.-M.; Park, S. Au Nanorings with Intertwined Triple Rings. *J. Am. Chem. Soc.* **2021**, *143* (37), 15113–15119.

(3) Pérez-Juste, J.; Pastoriza-Santos, I.; Liz-Marzán, L. M.; Mulvaney, P. Gold Nanorods: Synthesis, Characterization and Applications. *Coord. Chem. Rev.* **2005**, *249* (17), 1870–1901.

(4) Murphy, C. J.; Sau, T. K.; Gole, A. M.; Orendorff, C. J.; Gao, J.; Gou, L.; Hunyadi, S. E.; Li, T. Anisotropic Metal Nanoparticles: Synthesis, Assembly, and Optical Applications. *J. Phys. Chem. B* **2005**, *109* (29), 13857–13870.

(5) Zheng, J.; Cheng, X.; Zhang, H.; Bai, X.; Ai, R.; Shao, L.; Wang, J. Gold Nanorods: The Most Versatile Plasmonic Nanoparticles. *Chem. Rev.* **2021**, *121* (21), 13342–13453.

(6) Jin, R.; Liu, C.; Zhao, S.; Das, A.; Xing, H.; Gayathri, C.; Xing, Y.; Rosi, N. L.; Gil, R. R.; Jin, R. Tri-icosahedral Gold Nanocluster $[Au_{37}(PPh_3)_{10}(SC_2H_4Ph)_{10}X_2]^+$: Linear

Assembly of Icosahedral Building Blocks. *ACS Nano* **2015**, *9* (8), 8530–8536.
(7) Qian, H.; Zhu, Y.; Jin, R. Size-Focusing Synthesis, Optical and Electrochemical Properties of Monodisperse $Au_{38}(SC_2H_4Ph)_{24}$ Nanoclusters. *ACS Nano* **2009**, *3* (11), 3795–3803.
(8) Li, Y.; Song, Y.; Zhang, X.; Liu, T.; Xu, T.; Wang, H.; Jiang, D.-e.; Jin, R. Atomically Precise Au_{42} Nanorods with Longitudinal Excitons for an Intense Photothermal Effect. *J. Am. Chem. Soc.* **2022**, *144* (27), 12381–12389.
(9) Takano, S.; Yamazoe, S.; Koyasu, K.; Tsukuda, T. Slow-Reduction Synthesis of a Thiolate-Protected One-Dimensional Gold Cluster Showing an Intense Near-Infrared Absorption. *J. Am. Chem. Soc.* **2015**, *137* (22), 7027–7030.
(10) Zeng, C.; Chen, Y.; Li, G.; Jin, R. Magic Size $Au_{64}(S\text{-}c\text{-}C_6H_{11})_{32}$ Nanocluster Protected by Cyclohexanethiolate. *Chem. Mater.* **2014**, *26* (8), 2635–2641.
(11) Luo, L.; Liu, Z.; Kong, J.; Gianopoulos, C. G.; Coburn, I.; Kirschbaum, K.; Zhou, M.; Jin, R. Three-Atom-Wide Gold Quantum Rods with Periodic Elongation and Strongly Polarized Excitons. *Proc. Natl. Acad. Sci.* **2024**, *121* (10), e2318537121.
(12) Takahata, R.; Yamazoe, S.; Koyasu, K.; Tsukuda, T. Surface Plasmon Resonance in Gold Ultrathin Nanorods and Nanowires. *J. Am. Chem. Soc.* **2014**, *136* (24), 8489–8491.
(13) Takahata, R.; Tsukuda, T. Ultrathin Gold Nanowires and Nanorods. *Chem. Lett.* **2019**, *48* (8), 906–915.
(14) Li, Z.; Tao, J.; Lu, X.; Zhu, Y.; Xia, Y. Facile Synthesis of Ultrathin Au Nanorods by Aging the AuCl(oleylamine) Complex with Amorphous Fe Nanoparticles in Chloroform. *Nano Lett.* **2008**, *8* (9), 3052–3055.
(15) Morita, C.; Tanuma, H.; Kawai, C.; Ito, Y.; Imura, Y.; Kawai, T. Room-Temperature Synthesis of Two-Dimensional Ultrathin Gold Nanowire Parallel Array with Tunable Spacing. *Langmuir* **2013**, *29* (5), 1669–1675.
(16) Nakagawa, M.; Kawai, T. Chirality-Controlled Syntheses of Double-Helical Au Nanowires. *J. Am. Chem. Soc.* **2018**, *140* (15), 4991–4994.
(17) Takahata, R.; Yamazoe, S.; Koyasu, K.; Imura, K.; Tsukuda, T. Gold Ultrathin Nanorods with Controlled Aspect Ratios and Surface Modifications: Formation Mechanism and Localized Surface Plasmon Resonance. *J. Am. Chem. Soc.* **2018**, *140* (21), 6640–6647.
(18) Meyer, S. M.; Pettine, J.; Nesbitt, D. J.; Murphy, C. J. Size Effects in Gold Nanorod Light-to-Heat Conversion under Femtosecond Illumination. *J. Phys. Chem. C* **2021**, *125* (29), 16268–16278.
(19) Liu, T.-M.; Conde, J.; Lipiński, T.; Bednarkiewicz, A.; Huang, C.-C. Revisiting the Classification of NIR-Absorbing/Emitting Nanomaterials for in Vivo Bioapplications. *NPG Asia Mater.* **2016**, *8* (8), e295.
(20) Ah, C. S.; Hong, S. D.; Jang, D.-J. Preparation of $Au_{core}Ag_{shell}$ Nanorods and Characterization of Their Surface Plasmon Resonances. *J. Phys. Chem. B* **2001**, *105* (33), 7871–7873.
(21) Liu; Guyot-Sionnest, P. Synthesis and Optical Characterization of Au/Ag Core/Shell Nanorods. *J. Phys. Chem. B* **2004**, *108* (19), 5882–5888.
(22) Liu, X.; Astruc, D. From Galvanic to Anti-Galvanic Synthesis of Bimetallic Nanoparticles and Applications in Catalysis, Sensing, and Materials Science. *Adv. Mater.* **2017**, *29* (16), 1605305.
(23) Gan, Z.; Xia, N.; Wu, Z. Discovery, Mechanism, and Application of Antigalvanic Reaction. *Acc. Chem. Res.* **2018**, *51* (11), 2774–2783.
(24) Du, Y.; Sheng, H.; Astruc, D.; Zhu, M. Atomically Precise Noble Metal Nanoclusters as Efficient Catalysts: A Bridge between Structure and Properties. *Chem. Rev.* **2020**, *120* (2), 526–622.
(25) Khatun, E.; Pradeep, T. New Routes for Multicomponent Atomically Precise Metal Nanoclusters. *ACS Omega* **2021**, *6* (1), 1-16.
(26) Choi, J.-P.; Fields-Zinna, C. A.; Stiles, R. L.; Balasubramanian, R.; Douglas, A. D.; Crowe, M. C.; Murray, R. W. Reactivity of $[Au_{25}(SCH_2CH_2Ph)_{18}]^{1-}$ Nanoparticles with Metal Ions. *J. Phys. Chem. C* **2010**, *114* (38), 15890–15896.
(27) Wang, M.; Wu, Z.; Chu, Z.; Yang, J.; Yao, C. Chemico-Physical Synthesis of Surfactant- and Ligand-Free Gold Nanoparticles and Their Anti-Galvanic Reduction Property. *Chem. Asian J.* **2014**, *9* (4), 1006–1010.
(28) Pattadar, D. K.; Masitas, R. A.; Stachurski, C. D.; Cliffel, D. E.; Zamborini, F. P. Reversing the Thermodynamics of Galvanic Replacement Reactions by Decreasing the Size of Gold Nanoparticles. *J. Am. Chem. Soc.* **2020**, *142* (45), 19268–19277.
(29) Sudha, V.; Sangaranarayanan, M. V. Underpotential Deposition of Metals: Structural and Thermodynamic Considerations. *J. Phys. Chem. B* **2002**, *106* (10), 2699–2707.
(30) Personick, M. L.; Langille, M. R.; Zhang, J.; Mirkin, C. A. Shape Control of Gold Nanoparticles by Silver Underpotential Deposition. *Nano Lett.* **2011**, *11* (8), 3394–3398.
(31) Kang, H.; Kim, B.-G.; Na, H. B.; Hwang, S. Anti-Galvanic Reduction of Silver Ion on Gold and Its Role in Anisotropic Growth of Gold Nanomaterials. *J. Phys. Chem. C* **2015**, *119* (46), 25974-25982.
(32) Takahata, R.; Yamazoe, S.; Warakulwit, C.; Limtrakul, J.; Tsukuda, T. Rayleigh Instability and Surfactant-Mediated Stabilization of Ultrathin Gold Nanorods. *J. Phys. Chem. C* **2016**, *120* (30), 17006–17010.
(33) Takahata, R.; Yamazoe, S.; Koyasu, K.; Tsukuda, T. Structural Model of Ultrathin Gold Nanorods Based on High-Resolution Transmission Electron Microscopy: Twinned 1D Oligomers of Cuboctahedrons. *J. Phys. Chem. C* **2017**, *121* (20), 10942–10947.
(34) Crespo, J.; López-de-Luzuriaga, J. M.; Monge, M.; Elena Olmos, M.; Rodríguez-Castillo, M.; Cormary, B.; Soulantica, K.; Sestu, M.; Falqui, A. The Spontaneous Formation and Plasmonic Properties of Ultrathin Gold–Silver Nanorods and Nanowires Stabilized in Oleic Acid. *Chem. Commun.* **2015**, *51* (93), 16691–16694.
(35) Quintana, J.; Crespo, J.; Falqui, A.; López-de-Luzuriaga, J. M.; Olmos, M. E.; Rodríguez-Castillo, M.; Monge, M. Mini AuAg Wavy Nanorods Displaying Plasmon-Induced Photothermal and Photocatalytic Properties. *Adv. Photonics Res.* **2023**, *4* (2), 2200246.
(36) Imura, Y.; Mori, T.; Morita-Imura, C.; Kataoka, H.; Akiyama, R.; Kurata, H.; Kawai, T. Preparation and Length Control of Water-Dispersible Ultrathin Gold and Silver Bimetallic Nanowires. *Colloids and Surfaces A* **2018**, *543*, 9–14.
(37) Mulvaney, P.; Pérez-Juste, J.; Giersig, M.; Liz-Marzán, L. M.; Pecharromán, C. Drastic Surface Plasmon Mode Shifts in Gold Nanorods Due to Electron Charging. *Plasmonics* **2006**, *1* (1), 61–66.

For Table of Contents Only